Technology in Cancer Research & Treatment
ISSN 1533-0346
Volume 3, Number 1, February (2004)
Adenine Press

Nanoshell-Enabled Photonics-Based Imaging and Therapy of Cancer

www.tcrt.org

Christopher Loo, B.S.[1]
Alex Lin, B.S.[1]
Leon Hirsch, B.S.[1]
Min-Ho Lee, M.S.[1]
Jennifer Barton, Ph.D.[2]
Naomi Halas, Ph.D.[3]
Jennifer West, Ph.D.[1]
Rebekah Drezek, Ph.D.[1,*]

[1]Department of Bioengineering
Rice University
P.O. Box 1892, MS-142
Houston, TX 77030
[2]Biomedical Engineering Program
University of Arizona
1501 N. Campbell
P.O. Box 245084
Tucson, Arizona 85724
[3]Departments of Electrical and Computer Engineering
Rice University
P.O. Box 1892, MS-366
Houston, TX 77030

* Corresponding Author:
Rebekah Drezek, Ph.D.
Email: drezek@rice.edu

Metal nanoshells are a novel type of composite spherical nanoparticle consisting of a dielectric core covered by a thin metallic shell which is typically gold. Nanoshells possess highly favorable optical and chemical properties for biomedical imaging and therapeutic applications. By varying the relative the dimensions of the core and the shell, the optical resonance of these nanoparticles can be precisely and systematically varied over a broad region ranging from the near-UV to the mid-infrared. This range includes the near-infrared (NIR) wavelength region where tissue transmissivity peaks. In addition to spectral tunability, nanoshells offer other advantages over conventional organic dyes including improved optical properties and reduced susceptibility to chemical/thermal denaturation. Furthermore, the same conjugation protocols used to bind biomolecules to gold colloid are easily modified for nanoshells. In this article, we first review the synthesis of gold nanoshells and illustrate how the core/shell ratio and overall size of a nanoshell influences its scattering and absorption properties. We then describe several examples of nanoshell-based diagnostic and therapeutic approaches including the development of nanoshell bioconjugates for molecular imaging, the use of scattering nanoshells as contrast agents for optical coherence tomography (OCT), and the use of absorbing nanoshells in NIR thermal therapy of tumors.

Key words: Biophotonics, Contrast agents, Photothermal therapy, Nanotechnology.

Introduction

There is a significant clinical need for novel methods for detection and treatment of cancer which offer improved sensitivity, specificity, and cost-effectiveness. In recent years, a number of groups have demonstrated that photonics-based technologies are valuable in addressing this need. Optical technologies promise high resolution, noninvasive functional imaging of tissue at competitive costs. However, in many cases, these technologies are limited by the inherently weak optical signals of endogenous chromophores and the subtle spectral differences of normal and diseased tissue. Over the past several years, there has been increasing interest in combining emerging optical technologies with the development of novel exogenous contrast agents, designed to probe the molecular specific signatures of cancer, to improve the detection limits and clinical effectiveness of optical imaging. For instance, Sokolov *et al*. (1) recently demonstrated the use of gold colloid conjugated to antibodies to the epidermal growth factor receptor (EGFR) as scattering contrast agents for biomolecular optical imaging of cervical cancer cells and tissue specimens. In addition, optical imaging applications of nanocrystal bioconjugates have been described by multiple groups including Bruchez *et al*. (2), Chan and Nie (3), and Akerman *et al*. (4). More

Abbreviations: Near infrared (NIR), Optical coherence tomography (OCT), Polyethylene glycol (PEG)

recently, interest has developed in the creation of nanotechnology-based platform technologies which couple molecular specific early detection strategies with appropriate therapeutic intervention and monitoring capabilities.

Figure 1: Visual demonstration of the tunability of metal nanoshells.

Metal nanoshells are a new type of nanoparticle composed of a dielectric core such as silica coated with an ultrathin metallic layer, which is typically gold. Gold nanoshells possess physical properties similar to gold colloid, in particular, a strong optical absorption due to the collective electronic response of the metal to light. The optical absorption of gold colloid yields a brilliant red color which has been of considerable utility in consumer-related medical products, such as home pregnancy tests. In contrast, the optical response of gold nanoshells depends dramatically on the relative size of the nanoparticle core and the thickness of the gold shell. By varying the relative core and shell thicknesses, the color of gold nanoshells can be varied across a broad range of the optical spectrum that spans the visible and the near infrared spectral regions (Figure 1) (5, 6). Gold nanoshells can be made to either preferentially absorb or scatter light by varying the size of the particle relative to the wavelength of the light at their optical resonance. In Figure 2, a Mie scattering plot of the nanoshell plasmon resonance wavelength shift as a function of nanoshell composition for the case of a 60 nm

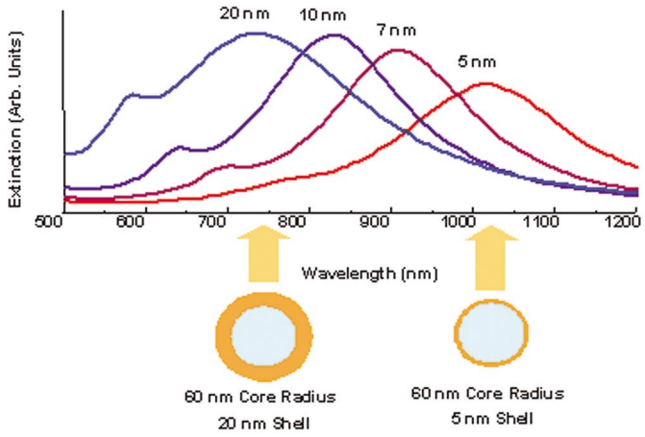

Figure 2: Optical resonances of gold shell-silica core nanoshells as a function of their core/shell ratio. Respective spectra correspond to the nanoparticles depicted beneath.

core gold/silica nanoshell is depicted. In this figure, the core and shell of the nanoparticles are shown to relative scale directly beneath their corresponding optical resonances. In Figure 3, a plot of the core/shell ratio versus resonance wavelength for a silica core/gold shell nanoparticle is displayed (6). The extremely agile "tunability" of the optical resonance is a property unique to nanoshells: in no other molecular or nanoparticle structure can the resonance of the optical absorption properties be so systematically "designed."

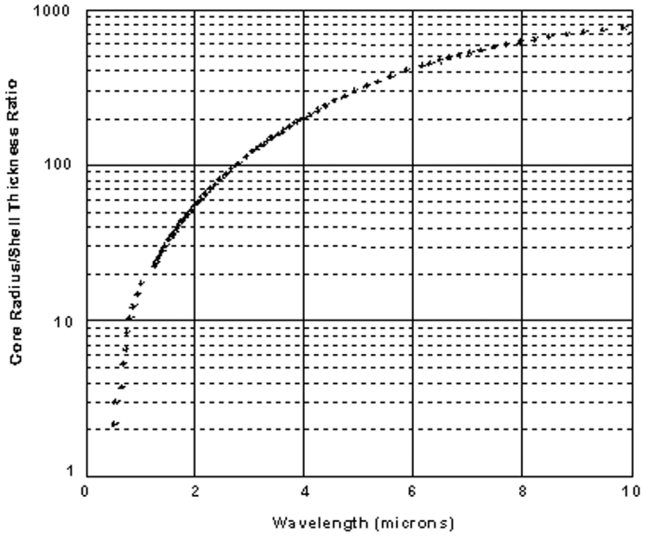

Figure 3: Core/shell ratio as a function of resonance wavelength for gold/silica nanoshells.

Halas and colleagues have completed a comprehensive investigation of the optical properties of metal nanoshells (7). Quantitative agreement between Mie scattering theory and the experimentally observed optical resonant properties has been achieved. Based on this success, it is now possible to predictively design gold nanoshells with the desired optical resonant properties and fabricate the nanoshell with the dimensions and nanoscale tolerances necessary to achieve these properties (6). The synthetic protocol developed for the fabrication of gold nanoshells is very simple in concept:

I. grow or obtain silica nanoparticles dispersed in solution,
II. attach very small (1-2 nm) metal "seed" colloid to the surface of the nanoparticles via molecular linkages; these seed colloids cover the dielectric nanoparticle surfaces with a discontinuous metal colloid layer,
III. grow additional metal onto the "seed" metal colloid adsorbates via chemical reduction in solution.

This approach has been successfully used to grow both gold and silver metallic shells onto silica nanoparticles. Various stages in the growth of a gold metallic shell onto a function-

alized silica nanoparticle are shown in Figure 4. Figure 5 shows the optical signature of shell coalescence and growth for two different nanoshell core diameters.

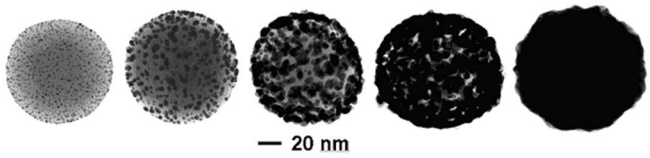

Figure 4: Transmission electron microscope images of gold/silica nanoshells during shell growth.

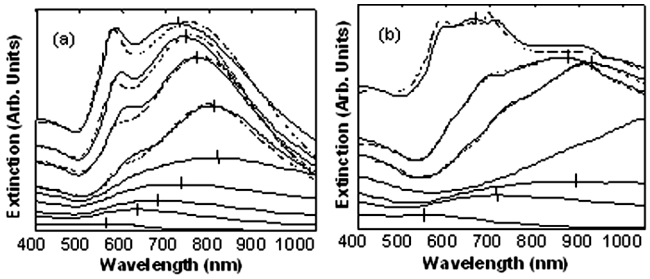

Figure 5: (**a**) Growth of gold shell on 120 nm diameter silica nanoparticle. The lower spectral curves follow the evolution of the optical absorption as coalescence of the gold layer progresses. Once the shell is complete, the peak absorbance is shifted to shorter wavelengths. Corresponding theoretical peaks are plotted with dashed lines. (**b**) Growth of gold shell on 340 nm diameter silica nanoparticles. Here the peak shifts are more pronounced with only the shoulder of the middle curve visible in our instrument range.

Based on the core/shell ratios that can be achieved with this protocol, gold nanoshells with optical resonances extending from the visible region to approximately 3 μm in the infrared can currently be fabricated. This spectral region includes the 800-1300 nm "water window" of the near infrared, a region of high physiological transmissivity which has been demonstrated as the spectral region best suited for optical bioimaging and biosensing applications. The optical properties of gold nanoshells, when coupled with their biocompatibility and their ease of bioconjugation, render these nanoparticles highly suitable for targeted bioimaging and therapeutic applications. By controlling the physical parameters of the nanoshells, it is possible to engineer nanoshells which primarily scatter light as would be desired for many imaging applications, or alternatively, to design nanoshells which are strong absorbers permitting photothermal-based therapy applications. The tailoring of scattering and absorption cross-sections is demonstrated in Figure 6 which shows sample spectra for two nanoshell configurations, one designed to scatter light and the other to preferentially absorb light.

Because the metal layer of gold nanoshells is grown using the same chemical reaction as gold colloid synthesis, the surfaces of gold nanoshells are virtually chemically identical to the surfaces of the gold nanoparticles universally used in bioconjugate applications. The use of gold colloid in bio-

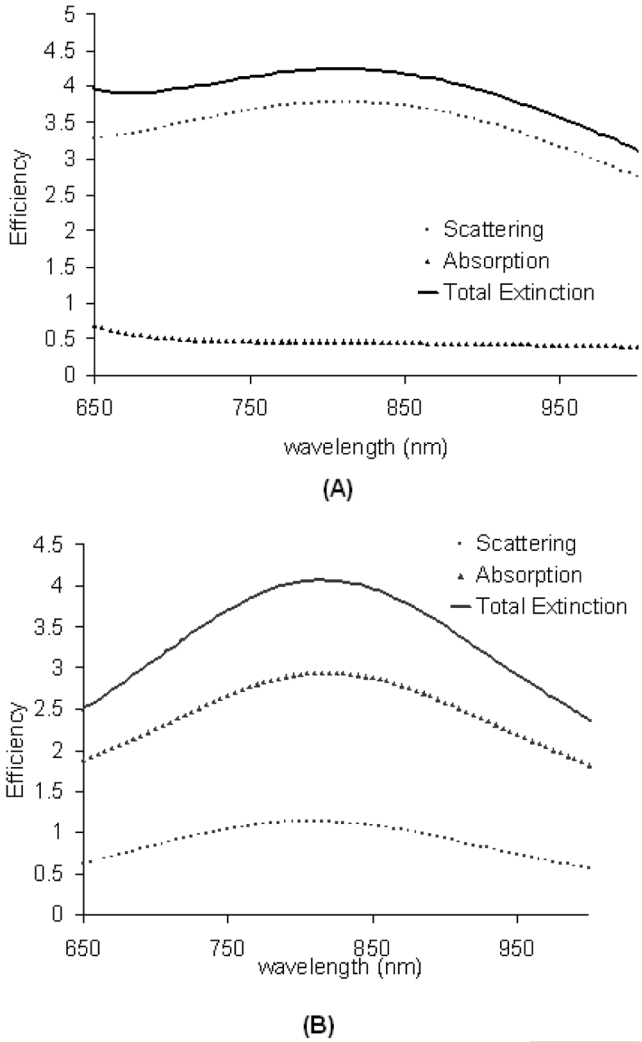

Figure 6: Nanoshells may be designed to be predominantly scattering or absorbing by tailoring the core and shell fabrication materials. To demonstrate this concept, the predicted scattering efficiency, absorption efficiency, and extinction are shown for two nanoshells: (**A**) a scattering configuration (core radius = 40 nm; shell thickness = 20 nm) (5) and (**B**) an absorbing configuration (core radius = 50 nm; shell thickness = 10 nm).

logical applications began in 1971 when Faulk and Taylor invented the immunogold staining procedure (8). Since that time, the labeling of targeting molecules, especially proteins, with gold nanoparticles has revolutionized the visualization of cellular or tissue components by electron microscopy. The optical and electron beam contrast qualities of gold colloid have provided excellent detection qualities for such techniques as immunoblotting, flow cytometry, and hybridization assays. Conjugation protocols exist for the labeling of a broad range of biomolecules with gold colloid, such as protein A, avidin, streptavidin, glucose oxidase, horseradish peroxidase, and IgG. Successful gold nanoshell conjugation with enzymes and antiobodies has previously been demonstrated.

In this article, we present data demonstrating the potential of nanoshells for several biomedical applications including the use of nanoshell bioconjugates as biological labels for optical imaging, the development of nanoshell-based scattering contrast agents for optical coherence tomography, and the use of absorbing nanoshells for photothermal therapy of tumors.

Methods and Materials

Gold Nanoshell Fabrication

Cores of silica nanoparticles were fabricated as described by Stober *et al*. (9) in which tetraethyl orthosilicate was reduced in NH_4OH in ethanol Particles were sized with a Philips XL30 scanning electron microscope. Polydispersity of <10% was considered acceptable. Next, the silica surface was aminated by reaction with aminopropyltriethoxysilane in ethanol. Gold shells were grown using the method of Duff *et al*. (10). Briefly, small gold colloid (1-3 nm) was adsorbed onto the aminated silica nanoparticle surface. More gold was then reduced onto these colloid nucleation sites using potassium carbonate and $HAuCl_4$ in the presence of formaldehyde. Gold nanoshell formation and dimensions were assessed with a UV-VIS spectrophotometer and scanning electron microscopy (SEM). The nanoshells used in the darkfield scattering imaging studies described consisted of a 120 nm silica core radius with a 35 nm thick gold shell. The nanoshells used in the OCT imaging consisted of a 100 nm core radius and 20 nm thick shell. The nanoshells used in the therapy application described used a 60 nm core radius and a 10 nm thick shell which absorb light with an absorption peak at ~815 nm. The reader is referred to (6) for a detailed description of nanoshell synthesis procedures.

Antibody Conjugation

Ortho-pyridyl-disulfide-*n*-hydroxysuccinimide polyethylene glycol polymer (OPSS-PEG-NHS, MW=2000) was used to tether antibodies onto the surfaces of gold nanoshells. Using $NaHCO_3$ (100 mM, pH 8.5) OPSS-PEG-NHS was re-suspended to a volume equal to that of either HER2 (specific) or IgG (non-specific) antibodies. At this concentration, the concentration of polymer was in molar excess to the amount of HER2 or IgG antibody used. The reaction was allowed to proceed on ice overnight. Excess, unbound polymer was removed by membrane dialysis (MWCO = 10,000). PEGylated antibody (0.67 mg/mL) was added to nanoshells (~10^9 nanoshells/mL) for 1 hr to facilitate targeting. Unbound antibody was removed by centrifugation at 650 G, supernatant removal, and resuspension in potassium carbonate (2 mM). Following antibody conjugation, nanoshells surfaces were further modified with PEG-thiol (MW=5000, 1 μM) to block non-specific adsorption sites and to enhance biocompatibility.

Cell Culture

HER2-positive SKBr3 human mammary adenocarcinoma cells were cultured in McCoy's 5A modified medium supplemented with 10% FBS and antibiotics. Cells were maintained at 37° C and 5% CO_2.

Molecular Imaging, Cytotoxicity, and Silver Staining

SKBR3 cells were exposed to 8 μg/mL of bioconjugated nanoshells for 1 hr, washed with phosphate-buffered saline, and observed under darkfield microscopy, a form of microscopy sensitive only to scattered light. The calcein-AM live stain (Molecular Probes, 1 μM) was used to assess cell viability after nanoshell targeting. A silver enhancement stain (Amersham Pharmacia), a qualitative stain capable of detecting the presence of gold on cell surfaces, was used to assess cellular nanoshell binding. Cells incubated with targeted nanoshells were fixed with 2.5% glutaraldehyde, and exposed to silver stain for 15 minutes. Silver growth was monitored under phase-contrast, with further silver enhancement blocked by immersion in 2.5% sodium thiosulfate. Darkfield and silver stain images were taken with a Zeiss Axioskop 2 plus microscope equipped with a black-white CCD camera. All images were taken at 40X magnification under the same lighting conditions.

Optical Coherence Tomograhy (OCT)

Optical coherent tomography (OCT) is a state-of-the-art imaging technique which produces high resolution (typically 10-15 μm), real-time, cross-sectional images through biological tissues. The method is often described as an optical analog to ultrasound. OCT detects the reflections of a low coherence light source directed into a tissue and determines at what depth the reflections occurred. By employing a heterodyne optical detection scheme, OCT is able to detect very faint reflections relative to the incident power delivered to the tissue. In OCT imaging out of focus light is strongly rejected due to the coherence gating inherent to the approach. This permits deeper imaging using OCT than is possible using alternative methods such as reflectance confocal microscopy where the out of focus rejection achievable is far lower. In the OCT experiments described in this paper, a conventional OCT system with an 830 nm superluminescent diode was used to obtain m-scans of the cuvette (images with time as the x-axis and depth as the y-axis). The axial and lateral resolution of the OCT system were 16 μm and 12 μm, respectively. Each image required approximately 20 seconds to acquire. System parameters remained the same throughout the experiment.

In Vitro Photothermal Nanoshell Therapy

SKBr3 breast cancer cells were cultured in 24-well plates until fully confluent. Cells were then divided into two treat-

ment groups: nanoshells + NIR-laser and NIR-laser alone. Cells exposed to nanoshells alone or cells receiving neither nanoshells nor laser were used as controls. Nanoshells were prepared in FBS-free medium (2×10^9 nanoshells/mL). Cells were then irradiated under a laser emitting light at 820 nm at a power density of ~35 W/cm^2 for 7 minutes with or without nanoshells. After NIR-light exposure, cells were replenished with FBS-containing media and were incubated for an additional hour at 37° C. Cells were then exposed to the calcein-AM live stain for 45 minutes in order to measure cell viability. The calcein dye causes viable cells to fluoresce green. Fluorescence was visualized with a Zeiss Axiovert 135 fluorescence microscope equipped with a filter set specific for excitation and emission wavelengths at 480 and 535 nm, respectively. Membrane damage was assessed using an aldehyde-fixable fluorescein dextran dye. Cells were incubated for 30 min with the fluorescent dextran, rinsed, and immediately fixed with 5% glutaraldehyde. Photothermal destruction of cells was attributed to hyperthermia induced via nanoshell absorption of NIR light.

Results and Discussion

As an initial demonstration of the potential of nanoshells in cancer imaging and therapy, we designed and fabricated nanoshells suitable for both scattering and absorption-based photonics applications. For proof-of-principle imaging studies, we fabricated nanoshells with a 120 nm radius and 35 nm shell thickness. It should be noted that nanoshells over a broad range of sizes can be fabricated for scattering based imaging applications. Figure 7 displays the predicted scattering and absorption spectra for these nanoshells obtained using software extensively verifed against Mie theory which numerically computes optical spectra for gold nanoshells.

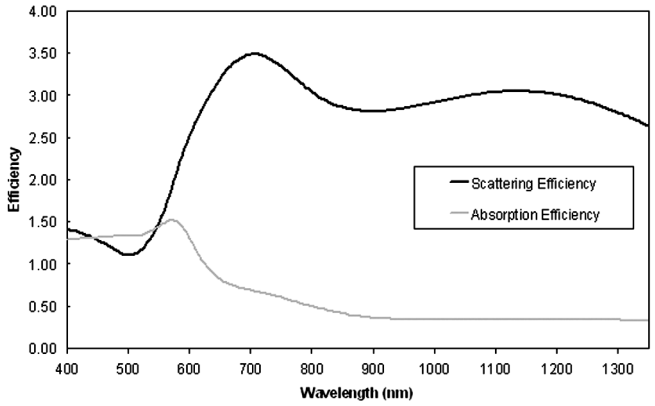

Figure 7: Scattering and absorbing properties of nanoshells with a 120 nm silica core radius and a 35 nm thick gold shell predicted analytically. Scattering maximum (705-710 nm) is 2.5-times greater than absorption maximum (570 nm) and extends into the NIR region. Nanoshell dimensions were assessed using scanning electron microscopy (SEM). Shell thickness was mathematically corroborated by matching experimental measurements to scattering theory and confirmed with SEM.

As Figure 7 demonstrates, these nanoshells scatter light strongly throughout the visible and near-infrared regions. This permits the same nanoshells to be used in light-based microscopy studies employing silicon CCDs and in NIR tissue imaging studies using reflectance confocal microscopy and OCT. We also fabricated nanoshells with a 100 nm radius and 20 nm shell thickness for OCT imaging. These nanoshells have very similar scattering and absorption spectra to the larger nanoshells; however, the scattering and absorption cross-sections are smaller due largely to the smaller particle size. In addition, smaller 60 nm radius

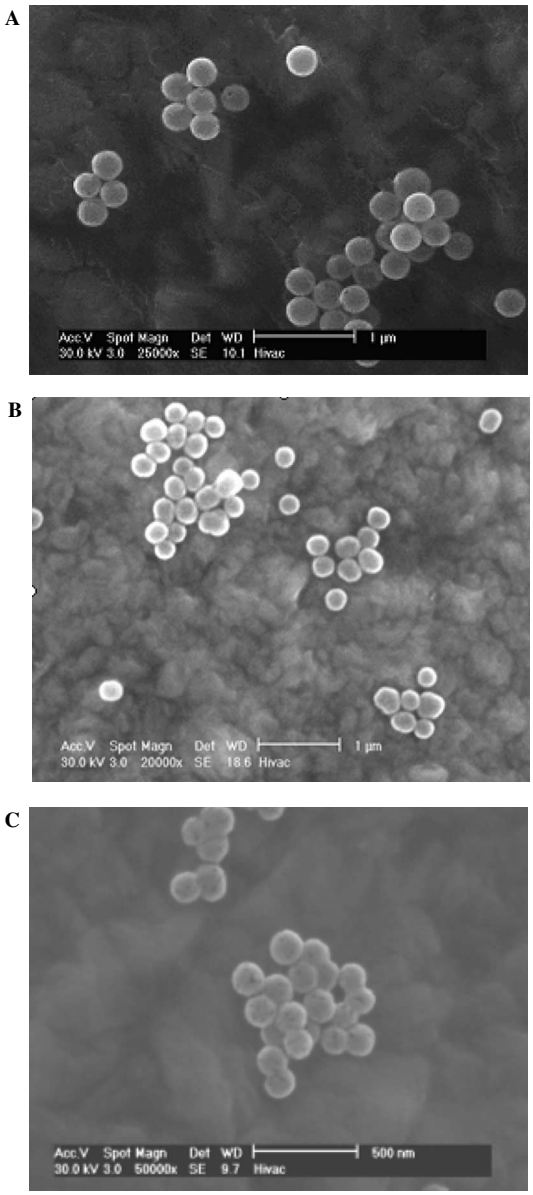

Figure 8: SEM images of nanoshells used in the described studies. The top image (**A**) shows the larger diameter nanoshells used in the darkfield imaging experiments. The middle image (**B**) shows the nanoshells used in the OCT experiments. The bottom image (**C**) show the smaller diameter nanoshells used for photothermal therapy applications. The scale bars in (**A**) and (**B**) are 1 µm while the scale bar in (**C**) is 500 nm.

nanoshells with a 10 nm shell were fabricated for photothermal therapy applications. Figure 8 shows SEM images of the nanoshells fabricated at all three sizes.

As an initial demonstration of the molecular imaging potential of nanoshell bioconjugates, we imaged carcinoma cells which overexpress HER2, a clinically significant molecular marker of breast cancer. Under darkfield microscopy, a form of microscopy sensitive only to scattered light, significantly increased optical contrast due to HER2 expression was observed in HER2-positive SKBR3 breast cancer cells targeted with HER2-labeled nanoshells compared to cells targeted by nanoshells non-specifically labelled with IgG (Figure 9). In addition, greater silver staining intensity was seen in cells exposed to HER2-targeted nanoshells than cells exposed to IgG-targeted nanoshells, providing additional evidence that the increased contrast seen under darkfield may be specifically attributable to nanoshell targeting of the HER2 receptor. No differences were observed under darkfield or silver stain in HER2 and IgG-targeted nanoshells using the HER2-negative MCF7 breast cancer cell line (data not shown). More extensive descriptions of imaging experiments using nanoshell bioconjugates are described in (11).

Although darkfield microscopy is suitable for *in vitro* cell level imaging experiments, *in vivo* imaging applications will require the use of appropriate scattering-based imaging technologies such as optical coherence tomography (OCT). To assess the suitability of nanoshells for OCT applications, we computed the scattering efficiencies of gold nanoshells (in saline) over a range of core radii and shell thicknesses at 830 nm as shown in Figure 10. The promising scattering cross-sections (approximately several times the geometric cross-sections) computed for nanoshells based on physical parameters which could be readily fabricated encouraged further experimental investigation. To provide a basis for comparison of scattering efficiencies, a 150 nm diameter polystytene sphere in saline at 830 nm has a scattering efficiecy of 0.009; a 300 nm polystyrene sphere has an efficiency of 0.09. As a visual demonstration of the potential of nanoshells for OCT imaging applications, we imaged a 1 mm pathlength cuvette containing one of three solutions: saline, a microsphere-based scattering solution, or a solution of scattering nanoshells in water (Figure 10). The microsphere mixture was 0.1% solids by volume of 2 μm polystyrene spheres in saline at a concentration which provided a scattering coefficient, $\mu_{s,} = 16\ cm^{-1}$ and an anisotropy factor, g = 0.96. The nanoshell (100 nm radius/20 nm shell) concentration was approximately 10^9/mL. Figure 10 shows OCT images of the cuvette with saline, microspheres and nanoshells. The images consist of one hundred scans in the same lateral location. The average grayscale value inside the cuvette walls was calculated using the NIH Image Analysis Program. The OCT intensity is based on a log scale where black (255) corresponds to the noise floor of -100 dB and white (0) to -40 dB. The average grayscale intensity for saline was 247 while the average intensity within the cuvette walls containing nanoshells the intensity was 160. Current efforts are more carefully exploring the potential of nanoshells as contrast agents for OCT through *in vivo* imaging studies of mice after direct injection of scattering nanoshells into the vasculature via a tail vein catheter (12).

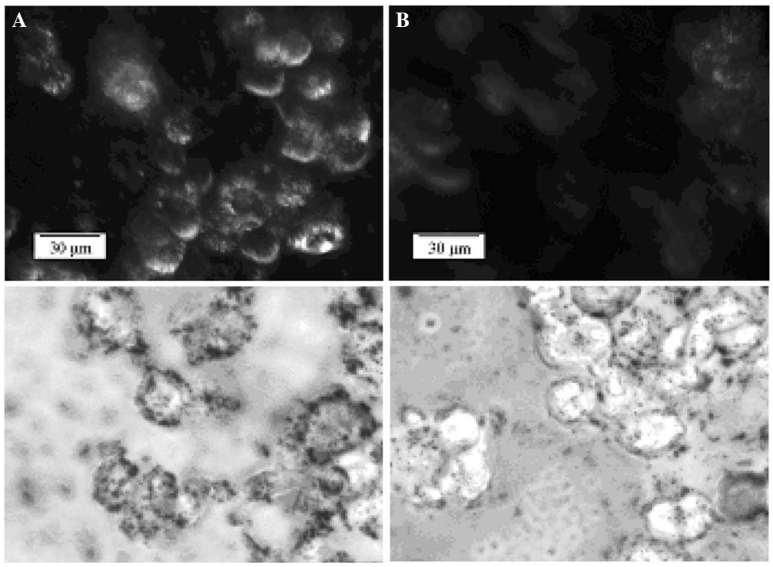

Figure 9: Darkfield (**top row**) and silver stain (**bottom row**) images of HER2-positive SKBR3 breast cancer cells exposed to nanoshells conjugated with either (**A**) HER2 (specific) or (**B**) IgG (non-specific) antibodies. As demonstrated here, it is possible to exploit the optical properties of predominantly-scattering nanoshells to image overexpressed HER2 in living cells. Similar scattering intensities were observed when comparing cells exposed to IgG-targeted nanoshells and cells not exposed to nanoshell bioconjugates.

Currently, our efforts are directed towards coupling our nanoshell-based molecular imaging technologies to some form of triggerable therapeutic intervention. Recent studies have considered a novel approach to cancer therapy based on the use of metal nanoshells as near-infrared (NIR) absorbers (13). In biological tissue, tissue transmissivity is highest in the NIR spectral range due to low inherent scattering and absorption properties within the region. Figure 7 demonstrates that nanoshells can be developed to highly scatter within this spectral regions; alternatively, nanoshells may be engineered to function as highly effective NIR absorbers as well. As an example of the intense absorption possible using nanoshells, the coventional NIR dye indocyanine green has an absorption cross-section of $\sim 10^{-20}\ m^2$ at ~800 nm while the cross-section of the absorbing nanoshells described in this article is $\sim 4 \times 10^{-14}\ m^2$, an approximately millionfold increase in absorption cross-section (13). By combining NIR absorbing nanoshells with an appropri-

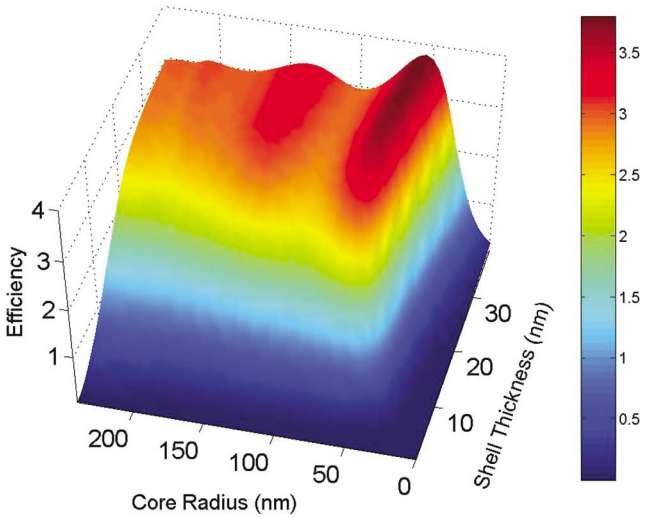

Figure 10: Computed scattering efficiency for nanoshells as a function of core radius and shell thickness at 830 nm, a wavelength commonly used in OCT imaging applications.

ate light source, it is possible to selectively induce photothermal destruction of cells and tumors treated with gold nanoshells. Nanoshell-mediated photothermal destruction of carcinoma cells is demonstrated in Figure 12. After laser exposure of 35 W/cm^2 for 7 minutes, all cells within the laser spot underwent photothermal destruction as assessed using calcein AM viability staining, an effect that was not observed in cells exposed to either nanoshells alone or NIR light alone. In addition, evidence of irreversible cell membrane damage was noted via imaging of the fluorescent dextran dye (date not shown). This dye is normally impermeable to healthy cells. However, the dye was found in the intracellular space of cells exposed to both NIR nanoshells and the laser but was not observed in cells exposed to either the NIR nanoshells or the laser alone. The calcein AM stain and the fluorescent dextran stain can be used to indicate that the cells are not viable and that membrane damage has occurred but do not determine the underlying cause of cell death.

In an animal study described in (13), absorbing nanoshells (10^9/ml, 20-50 µl) were injected interstially (~5 mm) into solid tumors (~1 cm) in female SCID mice. Within thirty minutes of injection, tumor sites were exposed to NIR light (820 nm, 4 W/cm^2, 5 mm spot diameter, <6 min). Temperatures were monitored via phase-sensitive, phase-spoiled gradient-echo MRI. Magnetic resonance temperature imaging (MRTI) demonstrated that tumors reached temperatures which caused irreversible tumor damage (ΔT = 37.4 ± 6.6° C) within 4-6 minutes. Controls which were exposed to a saline injection rather than nanoshells experienced significantly reduced average temperatures after exposure to the same NIR light levels ($\Delta T < 10^o$ C). These average temperatures were obtained at a depth of ~2.5 mm below the surface. The MRTI findings demonstrated good agreement with gross pathology indications of tissue damage. Histological indications of thermal damage including coagulation, cell shrinkage, and loss of nuclear staining were noted in nanoshell-treated tumors; no such changes were found in

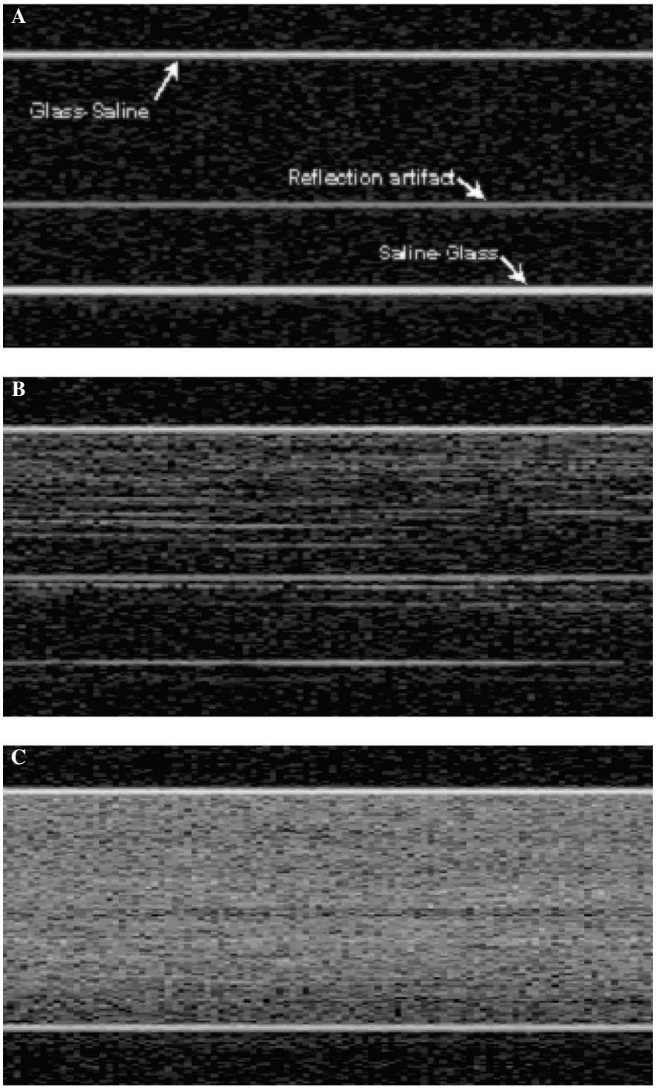

Figure 11: OCT (830 nm) images of a cuvette filled with saline (**A**), cuvette containing microspheres to approximate a scattering coefficient of 16 cm^{-1} (**B**), and cuvette containing nanoshells at a concentration of ~10^9/ml (**C**).

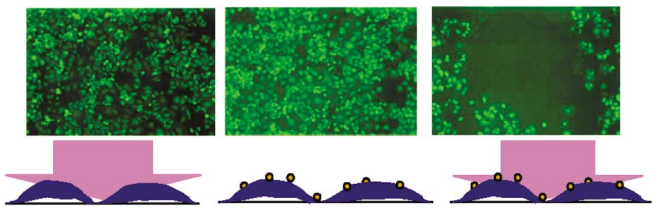

Figure 12: Calcein AM staining of cells (green fluorescence indiciates cellular viability). **Left:** cells after exposure to laser only (no nanoshells). **Middle:** cells incubated with nanoshells but not exposed to laser light. **Right:** cell incubated with nanoshells after laser exposure. The dark circle seen in the image on the right corresponds to the region of cell death caused by exposure to laser light after incubation with nanoshells.

control tissue. Silver enhancement staining provided further evidence of nanoshells in regions with thermal damage. The intial work described here established nanoshell and laser dosages which provided effective nanoshell-mediated photothermal therapy. Based on the parameters identified through these intial investigations, survival studies are now underway. Future work will also consider nanoshells conjugated to surface markers overexpressed within tumors.

Conclusions

Combining advances in biophotonics and nanotechnology offers the opportunity to significantly impact future strategies towards the detection and therapy of cancer. Today, cancer is typically diagnosed many years after it has developed usually after the discovery of either a palpable mass or based on relatively low resolution imaging of smaller but still significant masses. In the future, it is likely that contrast agents targeted to molecular markers of disease will routinely provide molecular information that enables characterization of disease susceptibility long before pathologic changes occur at the anatomic level. Currently, our ability to develop molecular contrast agents is at times constrained by limitations in our understanding of the earliest molecular signatures of specific cancers. Although the process of identifying appropriate targets for detection and therapy is ongoing, there is a strong need to develop the technologies which will allow us to image these molecular targets *in vivo* as they are elucidated. In this article, we describe the optical properties and several emerging clinical applications of nanoshells, one class of nanostructures which may provide an attractive candidate for specific *in vivo* imaging and therapy applications. We have reviewed our preliminary work towards the development of nanoshell bioconjugates for molecular imaging applications and described an important new approach to photothermal cancer therapy. More extensive *in vivo* animal studies for both cancer imaging and therapy applications are currently underway in order to investigate both the potential and limitations of nanoshell technologies. Additional studies are in progress to more thoroughly assess the biodistribution and biocompatibility of nanoshells used in *in vivo* imaging and therapy applications. We believe there is tremendous potential for synergy between the rapidly developing fields of biophotonics and nanotechnology. Combining the tools of both fields – together with the latest advances in understanding the molecular origins of cancer – may provide a fundamentally new approach to detection and treatment of cancer, a disease responsible for over one quarter of all deaths in the United States today.

Acknowledgements

Funding for this project was provided by the National Science Foundation (BES 022-1544), the National Science Foundation Center for Biological and Environmental Nanotechnology (EEC-0118007), and the Department of Defense Congressionally Directed Medical Research Program (DAMD17-03-1-0384).

References

1. Sokolov, K., Follen, M., Aaron, J., Pavlova, I., Malpica, A., Lotan, R., and Richards-Kortum, R. Real-time Vital Optical Imaging of Precancer Using Anti-epidermal Growth Factor Receptor Antibodies Conjugated to Gold Nanoparticles. *Cancer Research 63*, 1999-2004 (2003).
2. Bruchez, M, Moronne, M, Gin, P, Weiss, S, and Alivisatos, A. P. Semiconductor Labels as Fluorescent Biological Labels. *Science 281*, 2013-2016 (1998).
3. Chan, W. C. W. and Nie, S. Quantum Dot Bioconjugates for Ultrasensitive Nonisotopic Detection. *Science 281*, 2016-2018 (1998).
4. Akerman, M. E., Chan, W., Laakkonen, P., Bhatia, S. N., and Ruoslahti, E. Nanocrystal Targeting *In Vivo*. *PNAS*. *99*, 12617-12621 (2002).
5. Brongersma, M. L. Nanoshells: Gifts in a Gold Wrapper. *Nature Materials 2*, 296-297 (2003).
6. Oldenburg, S. J., Averitt, R. D., Westcott, S. L., and Halas, N. J. Nanoengineering of Optical Resonances. *Chemical Physics Letters 288*, 243-247 (1998).
7. Averitt R. D., Sarkar D., and Halas N. J. Plasmon Resonance Shifts of Au-coated Au2S Nanoshells: Insights into Multicomponent Banoparticles Growth. *Phys*. *Rev*. *Letters 78*, 4217-4220 (1997).
8. Faulk, W. T., and Taylor G. An Immunocolloid Method for the Electron Microscope. *Immunochemistry 8*, 1081-1083 (1971).
9. Stober, W., Fink, A., and Bohn, E. Controlled Growth of Monodisperse Silica Spheres in the Micron Size Range. *Journal of Colloid and Interface Science 26*, 62-69 (1968).
10. Duff, D. G., Baiker, A., and Edwards, P. P. A New Hydrosol of Gold Clusters. 1. Formation and Particle Size Variation. *Langmuir 9*, 2301-2309 (1993).
11. Loo, C. H., Hirsch, L. R, West, J. L., Halas, N. J. & Drezek, R. A. Molecular Imaging in Living Cells Using Nanoshell Bionconjugates. *Nanoletters*. In review (2004).
12. Barton, J., Romanowski, M., Halas, N., and Drezek, R. Nanoshells as an OCT Contrast Agent. *Proceedings of SPIE 5316*. In press (2004).
13. Hirsch, L. R., Stafford, R. J., Bankson, J. A., Sershen, S. R., Rivera, B., Price, R. E., Hazle, J. D., Halas, N. J., and West, J. L. Nanoshell-mediated Near-infrared Thermal Therapy of Tumors Under Magnetic Resonance Guidance. *PNAS*. *100*, 13549-13554 (2003).

Date Received: December 22, 2003